

COMMUNICATION

P2-type Layered $\text{Na}_{0.67}\text{Cr}_{0.33}\text{Mg}_{0.17}\text{Ti}_{0.5}\text{O}_2$ for Na Storage Applications

Received 00th January 20xx,
Accepted 00th January 20xx

Raizo Umezawa,^a Tsuchiya Yuka,^b Toru Ishigaki,^c Hongahally Basappa Rajendra,^a and Naoaki Yabuuchi^{*a, d, e}

DOI: 10.1039/x0xx00000x

$\text{Na}_{0.67}\text{Cr}_{0.33}\text{Mg}_{0.17}\text{Ti}_{0.5}\text{O}_2$ with a P2-type layered structure has been synthesized and examined as a negative electrode material for rechargeable sodium batteries. The layered oxide delivers a reversible capacity of > 90 mAh g⁻¹, which corresponds to > 95% of the theoretical capacity with excellent cyclability for > 450 cycles.

Low-cost energy storage technology is indispensable to realize sustainable energy development, and rechargeable sodium batteries made from abundant elements are the promising candidate for this purpose.¹⁻⁶ Layered materials, *e.g.*, $\text{LiCo}_{1-x}\text{Ni}_x/2\text{Mn}_x/2\text{O}_2$ and graphite, are widely used for practical lithium battery applications, including electric vehicles. Graphite, which has a two-dimensional diffusion path for guest ions with high electronic conductivity associated with a conjugated carbon framework structure, is an ideal host structure for this purpose. First-stage graphite intercalation compound, in which all interlayer sites are filled by guest ions, is formed by electrochemical reduction in aprotic electrolyte solutions with Li salts,⁷ and the reaction proceeds with high reversibility. However, sodium ions cannot be inserted into graphite, which presumably originates from the thermodynamic limitation, and only a high stage graphite intercalation compound is formed by electrochemical reduction in aprotic electrolyte solutions with Na salts.⁸ Instead of graphite, hard carbon, which has different microporous structures,⁹ is used as a negative electrode material for sodium storage applications.^{10, 11} Na ions are reversibly accumulated in hard carbon with micropores in which quasi-metallic sodium is formed.¹² A gravimetric reversible capacity as the negative electrode material

reaches to > 300 mAh g⁻¹, which is comparable to that of graphite used for rechargeable lithium batteries.¹¹ Nevertheless, the sodium insertion voltage in hard carbon synthesized at higher temperatures is extremely close to the plating potential of metallic sodium (< 0.1 V), and this fact results in the difficulty to design rapid charge batteries with hard carbon without less resistive interphase.¹³ Rapid charge for hard carbon leads to metallic sodium plating at the surface of hard carbon, which inevitably sacrifices the battery safety.

Titanium-based oxides are also extensively studied as the potential negative electrode materials for sodium storage applications, including $\text{Na}_2\text{Ti}_3\text{O}_7$,¹⁴ $\text{Na}_2\text{Ti}_6\text{O}_{13}$,¹⁵ $\text{Na}_4\text{Ti}_5\text{O}_{12}$,¹⁶ TiO_2 ¹⁷ *etc.*¹⁸ Among the materials reported in literature, chromium substituted Ti-based layered oxides, P2-type $\text{Na}_{0.6}\text{Cr}_{0.6}\text{Ti}_{0.4}\text{O}_2$,¹⁹ and P3-type $\text{Na}_{0.58}\text{Cr}_{0.58}\text{Ti}_{0.42}\text{O}_2$ ²⁰ show excellent reversibility as negative electrode materials. Herein, the notations of P2 and P3 are used for the classification of layered structures proposed by Delmas.²¹ “P” denotes the environment of sodium ions between metal oxide layers, and sodium ions are located at “prismatic” sites for both P2 and P3 phases. Numbers “2” and “3” indicate the total numbers of metal oxide slabs in the unit cells. These layered structures with MO_2 (M = transition metal ions) slabs formed by edge-shared MO_6 octahedra provide superior in-plane conductivity for both ions and electrons.²² These Ti-based layered oxides are operable at a relatively lower operating voltage range (1.1 – 0.5 V vs. metallic Na) on the basis of $\text{Ti}^{3+}/\text{Ti}^{4+}$ redox reaction. The operating voltage is relatively low as $\text{Ti}^{3+}/\text{Ti}^{4+}$ redox reaction compared with a Li counterpart (for instance, operating voltage is 1.55 V vs. metallic Li for $\text{Li}_{4+x}\text{Ti}_5\text{O}_{12}$ with a spinel-type structure²³) and is high enough to avoid metallic Na deposition. However, the use of Cr, which is a relatively less-abundant element, must be reduced for Na battery applications. Recently, sodium deficient O3-type $\text{Na}_{0.67}\text{Mg}_{0.33}\text{Ti}_{0.67}\text{O}_2$ without Cr ions has been reported in literature.²⁴ Herein, “O” denotes that sodium ions are located at “octahedral” sites. However, MgO is a typical basic oxide, which easily reacts with acid, and therefore, excess substitution of Mg ions in the host structure would lower its chemical stability as electrode materials.

^a Department of Chemistry and Life Science, Yokohama National University, 79-5 Tokiwadai, Hodogaya-ku, Yokohama, Kanagawa 240-8501, Japan

^b Department of Applied Chemistry, Tokyo Denki University, Adachi, Tokyo 120-8551, Japan

^c Frontier Research Center for Applied Atomic Sciences, Ibaraki University, 162-1, Shirakata, Tokai, Naka, Ibaraki 319-1106, Japan

^d Advanced Chemical Energy Research Center, Yokohama National University, 79-5 Tokiwadai, Hodogaya-ku, Yokohama, Kanagawa 240-8501, Japan

^e Elements Strategy Initiative for Catalysts and Batteries, Kyoto University, f1-30 Goryo-Ohara, Nishikyo-ku, Kyoto 615-8245, Japan

E-mail: yabuuchi-naoaki-pw@ynu.ac.jp

Electronic Supplementary Information (ESI) available: [details of any supplementary information available should be included here]. See DOI: 10.1039/x0xx00000x

In this study, P2-type $\text{Na}_{0.67}\text{Cr}_{0.67}\text{Ti}_{0.33}\text{O}_2$ is targeted as the host structure of potential negative electrode materials, from which Cr^{3+} is bi-substituted by $\text{Mg}^{2+}/\text{Ti}^{4+}$ to reduce Cr contents in the

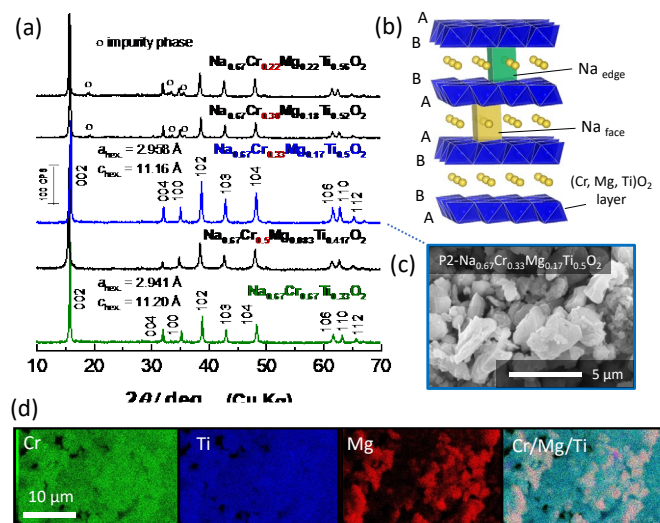


Figure 1. (a) XRD patterns of $\text{Na}_{0.67}\text{Cr}_{0.67-x}\text{Mg}_{x/2}\text{Ti}_{0.33+x/2}\text{O}_2$ with different chemical compositions. (b) A schematic illustration of the P2-type layered structure, which was drawn using the program, VESTA,²⁵ and (c) a SEM image and (d) EDX maps of $\text{Na}_{0.67}\text{Cr}_{0.33}\text{Mg}_{0.17}\text{Ti}_{0.50}\text{O}_2$ ($x = 0.33$ in $\text{Na}_{0.67}\text{Cr}_{0.67-x}\text{Mg}_{x/2}\text{Ti}_{0.33+x/2}\text{O}_2$) are also shown.

host structure. **Figure 1** shows X-ray diffraction (XRD) patterns of the samples prepared with different chemical compositions ($0.0 < x < 0.45$ in $\text{Na}_{0.67}\text{Cr}_{0.67-x}\text{Mg}_{x/2}\text{Ti}_{0.33+x/2}\text{O}_2$) in starting materials. Mixtures of Na_2CO_3 , Cr_2O_3 , $\text{Mg}(\text{OH})_2$, and TiO_2 (anatase form) were heated at $1000 \text{ }^\circ\text{C}$ for 5 h in Ar atmosphere (see Supplementary information in more detail), and the samples after heating were stored in an Ar-filled glove box to avoid the contact to moist air. Phase purity and crystal structures of the samples were studied using an X-ray diffractometer (D2 PHASER, Bruker) equipped with a high-speed one-dimensional detector. All measurements were conducted with an airtight sample holder to avoid air exposure. Structural analysis was conducted using RIETAN-FP software.²⁶ The P2-type layered structure is retained by $x \geq 0.33$ in $\text{Na}_{0.67}\text{Cr}_{0.67-x}\text{Mg}_{x/2}\text{Ti}_{0.33+x/2}\text{O}_2$ and a single phase of $\text{Na}_{0.67}\text{Cr}_{0.33}\text{Mg}_{0.17}\text{Ti}_{0.50}\text{O}_2$ is successfully synthesized by solid-state calcination. 50% of Cr ions are substituted by Mg/Ti ions from the original phase. Nevertheless, further reduction of Cr ions and enrichment of Mg/Ti ions result in the appearance of an impurity phase. $\text{O3-Na}_{0.67}\text{Mg}_{0.33}\text{Ti}_{0.67}\text{O}_2$ without Cr ions reported in literature²⁴ was not able to be synthesized by using our experimental conditions (see **Supporting Figure S1**). The impurity phase observed in **Figure 1a** is assigned into a Ti-based tunnel-type structure and is expected to be isostructural with CaFe_2O_4 -type structure,²⁷ in which Na and Cr/Mg/Ti ions presumably occupy Ca and Fe sites, respectively (see **Supporting Figure S2**). This impurity phase is enriched when the concentration of vacant sites is increased from 33% as shown in **Supporting Figure S2**.

Morphological features of $\text{Na}_{0.67}\text{Cr}_{0.33}\text{Mg}_{0.17}\text{Ti}_{0.50}\text{O}_2$ were observed using a scanning electron microscope (JCM-6000, JEOL) and

elemental maps for each ion were also obtained. Particles with the smooth faceted surface are observed (**Figure 1c**), which is originating from the synthesis condition; calcination at the higher temperature of $1000 \text{ }^\circ\text{C}$, and similar particle morphology is observed with the sample without Mg ions (**Supporting Figure S3**). Uniform distributions for Na, Cr, Mg, and Ti ions are also noted on elemental maps obtained by energy dispersive X-ray spectroscopy (**Figure 1d**), which is consistent with the data of XRD study.

Structural analysis of $\text{Na}_{0.67}\text{Cr}_{0.33}\text{Mg}_{0.17}\text{Ti}_{0.50}\text{O}_2$ was further conducted by time-of-flight neutron diffraction (TOF-ND) measurement at iMATERIA,²⁸ BL20 of Materials and Life Science Experimental Facility (MLF), J-PARC in Japan. The sample was sealed in a vanadium tube (6.0 mm in diameter) in an inert atmosphere. TOF-ND data was collected at room temperature. The collected data was analyzed using the Z-Rietveld software.²⁹ All diffraction lines were well fitted by using the structural model of the P2-type layered structure as shown in **Figure 2**. Refined structural parameters are also summarized in **Table 1**. Na ions are found at two distinct prismatic sites, $2b$ and $2d$ sites, and such trend is often observed for layered oxides with the P2-type structure.³⁰ Na ions at $2d$ prismatic sites share three edges with octahedral sites in the transition metal layer, which are expected to be energetically stable sites for Na ions. Na ions are also found at $2b$ prismatic sites, which share a face with the octahedral site in the transition metal layer, and thus larger repulsive electrostatic interaction is anticipated. Such unfavorable interaction at the face-shared site is partly relieved for the P2-type layered phase with a wide interlayer distance, and therefore Na ions are also found at $2b$ sites. From the neutron diffraction pattern, Cr and Ti ordering is not evidenced, which is also consistent with the

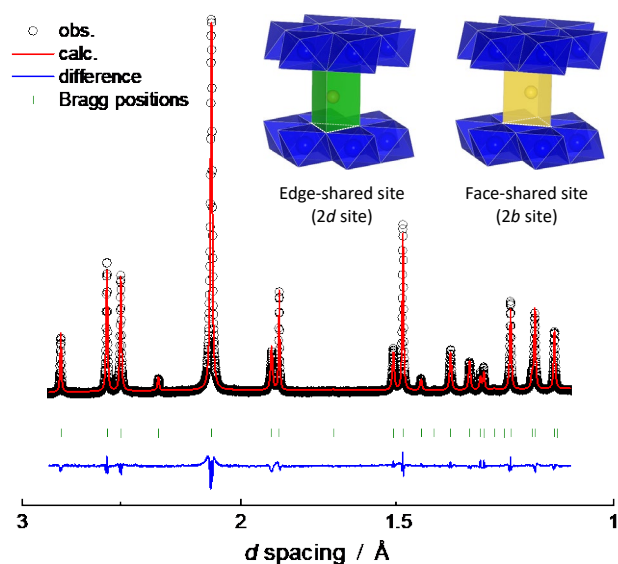


Figure 2. A refined result of Rietveld analysis on the neutron diffraction pattern of $\text{Na}_{0.67}\text{Cr}_{0.33}\text{Mg}_{0.17}\text{Ti}_{0.50}\text{O}_2$. Refined structural parameters are summarized in **Table 1**. Schematic illustrations of two distinct crystallographic sites, $2b$ and $2d$ sites, for Na ions are also shown.

former study without Mg ions.¹⁹ Na and vacancy ordering is also not evidenced on a synchrotron XRD pattern collected at SPring-8, BL19B2,²⁶ in Japan as shown in **Supporting Figure S4**.

Table 1. Crystallographic parameters obtained by Rietveld analysis on the neutron diffraction pattern of $\text{Na}_{0.67}\text{Cr}_{0.33}\text{Mg}_{0.17}\text{Ti}_{0.5}\text{O}_2$.

atom	site	<i>g</i>	<i>x</i>	<i>y</i>	<i>z</i>	<i>B</i> / Å ²
Na 1	2 <i>b</i>	0.183(2)	0	0	0.25	0.50(5)
Na 2	2 <i>d</i>	0.484(3)	1/3	2/3	0.75	0.50(5)
Cr	2 <i>a</i>	1/3	0	0	0	0.20(2)
Mg	2 <i>a</i>	1/6	0	0	0	0.20(2)
Ti	2 <i>a</i>	1/2	0	0	0	0.20(2)
O	4 <i>f</i>	1	1/3	2/3	0.093(1)	0.70(5)

Hexagonal, space group $P6_3/mmc$, $a = 2.9597(3)$ Å, $c = 11.169(1)$ Å, $V = 84.69$ Å³, $R_{\text{wp}} = 5.85\%$, $R_{\text{B}} = 3.74\%$

Electrochemical properties of $\text{Na}_{0.67}\text{Cr}_{0.33}\text{Mg}_{0.17}\text{Ti}_{0.5}\text{O}_2$ was tested in Na cells and the results are compared with those of $\text{Na}_{0.67}\text{Cr}_{0.66}\text{Ti}_{0.37}\text{O}_2$ without Mg ions in **Figure 3**. Electrode performance of the samples was examined in Na cells. The composite electrodes consisted of 80 wt% $\text{Na}_{0.67}\text{Cr}_{0.33}\text{Mg}_{0.17}\text{Ti}_{0.5}\text{O}_2$, 10 wt% acetylene black, and 10 wt% poly(vinylidene fluoride), pasted on aluminum foil as a current collector. Metallic sodium was used as a counter electrode. Electrolyte solution used was 1.0 mol dm⁻³ NaPF₆ in propylene carbonate (PC) with/without fluoroethylene carbonate (FEC) additive (Battery grade, Kishida Chemical).³¹ NaPF₆/PC electrolyte solution is known to be stable against metallic Na.³² Detailed experimental methodology of electrochemical characterization is described in literature.²⁰ The cell was cycled in the range of 0.2 – 2.0 V vs. metallic Na. Although Cr³⁺ is oxidized into highly toxic Cr⁶⁺ on charge to 4 V,²⁰ the possibility of the formation of Cr⁶⁺ is eliminated in this voltage range. Because the mass of Mg²⁺ is smaller than that of Cr³⁺, the substitution of Mg²⁺ for Cr³⁺ increases the theoretical capacity as negative electrode materials. Indeed, the increase in a reversible capacity (approximately 10 mA h g⁻¹) is noted for the Mg substituted sample (**Figure 3a**). No capacity fading is observed for the 50-cycle test as shown in **Figure 3b**. The observed reversible capacity at a rate of 10 mA g⁻¹ nearly corresponds to the theoretical capacity of $\text{Na}_{0.67}\text{Cr}_{0.33}\text{Mg}_{0.17}\text{Ti}_{0.5}\text{O}_2$ (96 mA h g⁻¹), which is estimated on the assumption that 1/3 mol of Na ions are reversibly inserted/extracted into/from $\text{Na}_{0.67+y}\text{Cr}_{0.33}\text{Mg}_{0.17}\text{Ti}_{0.5}\text{O}_2$. The voltage profiles are similar (1.1 – 0.5 V vs. Na metal) for both samples (**Figure 3c**), but a slightly broadened profile compared with the sample without Mg ions is noted in differential capacity plots (**Figure 3d**). Mg substitution for Cr/Ti ions influences phase transition processes, and thus clear voltage plateaus at 0.55 and 0.60 V on reduction and oxidation, respectively, observed for the non-substituted sample are lost. Moreover, the sample shows excellent rate capability and delivers a reversible capacity of > 60 mA h g⁻¹ even at a rate of 2560 mA g⁻¹ (**Figure 3e**). Rate capability of $\text{Na}_{0.67}\text{Cr}_{0.33}\text{Mg}_{0.17}\text{Ti}_{0.5}\text{O}_2$ is comparable to that of the non-substituted sample (**Supporting Figure S5**), and the deterioration of electrode performance is not caused by partial Mg substitution. The extended cycle test was also conducted for $\text{Na}_{0.67}\text{Cr}_{0.33}\text{Mg}_{0.17}\text{Ti}_{0.5}\text{O}_2$, and the sample was cycled for continuous 300 cycles at a rate of 100 mA g⁻¹ (**Figure 3f**). Although

the degradation is observed after 200 cycles in the electrolyte without FEC (**Supporting Figure S6**), good capacity retention without degradation is realized for > 450 cycles at a rate of 100 mA g⁻¹ as shown in **Figure 3f**. Similar capacity retention is also observed for P2 $\text{Na}_{0.67}\text{Cr}_{0.67}\text{Ti}_{0.33}\text{O}_2$ without Mg ions. Excellent capacity retention for the sample is expected to originate from a quite small volume change (approximately 1%) on electrochemical cycles. The original unit cell volume of 84.81 Å³ changes to 84.12 Å³ after sodium insertion as shown in **Supporting Figure S7**, and this process is highly reversible process. Further optimization of particle morphology, electrolyte, binders etc. will result in the further improvement of electrochemical properties of Ti-based layered oxides. These research progresses lead to the development of cost-effective and high-performance Na-ion batteries with moderate energy density in the future.

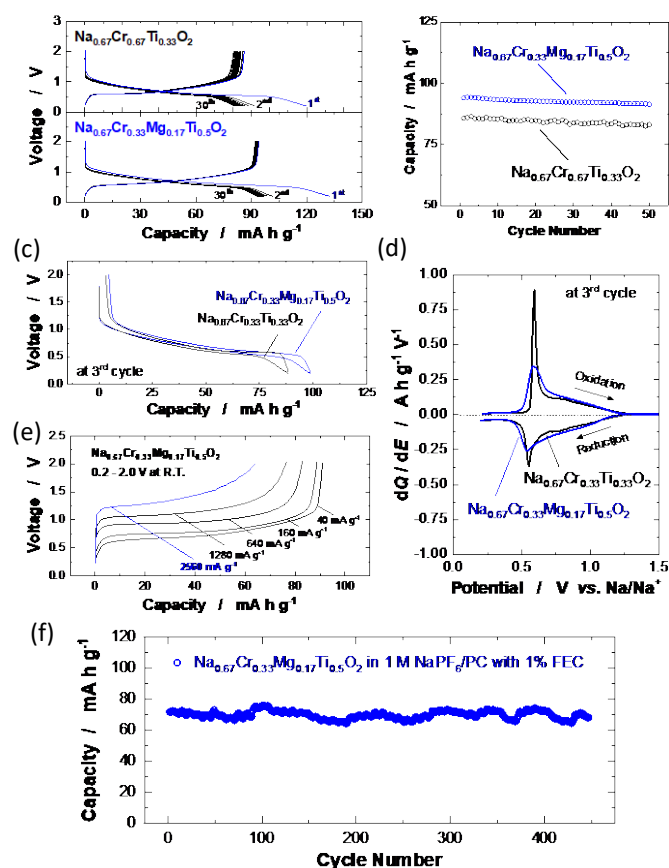


Figure 3. Electrochemical properties of $\text{Na}_{0.67}\text{Cr}_{0.33}\text{Mg}_{0.17}\text{Ti}_{0.5}\text{O}_2$ and $\text{Na}_{0.67}\text{Cr}_{0.67}\text{Ti}_{0.33}\text{O}_2$ as potential negative electrode materials for Na-ion batteries; (a) charge/discharge curves of the sample and (b) capacity retention at a rate of 10 mA g⁻¹. (c) Comparison of small hysteresis for charge/discharge processes (10 mA g⁻¹) obtained at 3rd cycle for both samples, and (d) differential capacity plots obtained from (c). Rate-capability of $\text{Na}_{0.67}\text{Cr}_{0.33}\text{Mg}_{0.17}\text{Ti}_{0.5}\text{O}_2$ is also evaluated as shown in (e). Sample loading was 4.73 mg/cm². (d) The extended cycle test in a Na cell with 1 vol% FEC additive at a rate of 100 mA g⁻¹. Specific capacities of the active materials were calculated on the basis of mass of layered oxides (80 wt%) in composite electrodes.

This work has been partially supported by JSPS, Grant-in-Aid for Scientific Research (Grant Numbers 15H05701, 19H05816, and

19K22229), and MEXT program “Elements Strategy Initiative to Form Core Research Center (JPMXP0112101003)”, MEXT; Ministry of Education Culture, Sports, Science and Technology, Japan. The synchrotron radiation experiments were performed at the BL19B2 of SPring-8 with the approval of the Japan Synchrotron Radiation Research Institute (JASRI) (Proposal 2019B1685). The ND experiments at the Materials and Life Science Experimental Facility of the J-PARC were performed under a user program (Proposal No. 2019PM2004).

Conflicts of interest

There are no conflicts to declare.

Notes and references

- B. Dunn, H. Kamath and J.-M. Tarascon, *Science*, 2011, **334**, 928-935.
- M. D. Slater, D. Kim, E. Lee and C. S. Johnson, *Adv. Funct. Mater.*, 2012, **23**, 947-958.
- J. M. Clark, P. Barpanda, A. Yamada and M. S. Islam, *J. Mater. Chem. A*, 2014, **2**, 11807-11812.
- N. Yabuuchi, *Chem. Rec.*, 2019, **19**, 690-707.
- T. Ando, S. Yubuchi, A. Sakuda, A. Hayashi and M. Tatsumisago, *Electrochemistry*, 2019, **87**, 289-293.
- T. Kobayashi, W. Zhao, H. B. Rajendra, K. Yamanaka, T. Ohta and N. Yabuuchi, *Small*, 2020, **16**, 1902462.
- T. Ohzuku, Y. Iwakoshi and K. Sawai, *J. Electrochem. Soc.*, 1993, **140**, 2490-2498.
- Y. Kondo, T. Fukutsuka, K. Miyazaki, Y. Miyahara and T. Abe, *J. Electrochem. Soc.*, 2019, **166**, A5323-A5327.
- S. Shimizu, H. B. Rajendra, R. Watanuki and N. Yabuuchi, *Electrochemistry*, 2019, **87**, 276-280.
- E. Irisarri, A. Ponrouch and M. R. Palacin, *J. Electrochem. Soc.*, 2015, **162**, A2476-A2482.
- K. Kubota, S. Shimadzu, N. Yabuuchi, S. Tominaka, S. Shiraishi, M. Abreu-Sepulveda, A. Manivannan, K. Gotoh, M. Fukunishi, M. Dahbi and S. Komaba, *Chem. Mater.*, 2020, **32**, 2961-2977.
- V. L. Deringer, C. Merlet, Y. Hu, T. H. Lee, J. A. Kattirtzi, O. Pecher, G. Csányi, S. R. Elliott and C. P. Grey, *Chem. Commun.*, 2018, **54**, 5988-5991.
- Y. Morikawa, Y. Yamada, K. Doi, S. Nishimura and A. Yamada, *Electrochemistry*, 2020, **88**, 151-156.
- P. Senguttuvan, G. I. Rousse, V. Seznec, J.-M. Tarascon and M. R. Palacin, *Chem. Mater.*, 2011, **23**, 4109-4111.
- A. Rudola, K. Saravanan, S. Devaraj, H. Gong and P. Balaya, *Chem. Commun.*, 2013, **49**, 7451-7453.
- P. J. P. Naeyaert, M. Avdeev, N. Sharma, H. B. Yahia and C. D. Ling, *Chem. Mater.*, 2014, **26**, 7067-7072.
- H. Usui, Y. Domi, S. Yoshioka, K. Kojima and H. Sakaguchi, *ACS Sustain. Chem. Eng.*, 2016, **4**, 6695-6702.
- R. Fielden and M. N. Obrovac, *J. Electrochem. Soc.*, 2014, **161**, A1158-A1163.
- Y. Wang, R. Xiao, Y.-S. Hu, M. Avdeev and L. Chen, *Nat. Commun.*, 2015, **6**.
- Y. Tsuchiya, K. Takanashi, T. Nishinobo, A. Hokura, M. Yonemura, T. Matsukawa, T. Ishigaki, K. Yamanaka, T. Ohta and N. Yabuuchi, *Chem. Mater.*, 2016, **28**, 7006-7016.
- C. Delmas, C. Fouassier and P. Hagemuller, *Physica B & C*, 1980, **99**, 81-85.
- N. Yabuuchi and S. Komaba, *Sci. Technol. Adv. Mater.*, 2014, **15**, 043501.
- T. Ohzuku, A. Ueda and N. Yamamoto, *J. Electrochem. Soc.*, 1995, **142**, 1431-1435.
- C. Zhao, M. Avdeev, L. Chen and Y.-S. Hu, *Angew. Chem.*, 2018, **57**, 7056-7060.
- K. Momma and F. Izumi, *J. Appl. Crystallogr.*, 2011, **44**, 1272-1276.
- F. Izumi and K. Momma, *Solid State Phenom.*, 2007, **130**, 15-20.
- H. Müller-Buschbaum and D. Frerichs, *J. Alloys Compd.*, 1993, **199**, L5-L8.
- T. Ishigaki, A. Hoshikawa, M. Yonemura, T. Morishima, T. Kamiyama, R. Oishi, K. Aizawa, T. Sakuma, Y. Tomota, M. Arai, M. Hayashi, K. Ebata, Y. Takano, K. Komatsuzaki, H. Asano, Y. Takano and T. Kasao, *Nucl. Instrum. Methods Phys. Res., Sect. A*, 2009, **600**, 189-191.
- R. Oishi, M. Yonemura, Y. Nishimaki, S. Torii, A. Hoshikawa, T. Ishigaki, T. Morishima, K. Mori and T. Kamiyama, *Nucl. Instrum. Methods Phys. Res. A*, 2009, **600**, 94-96.
- W. Zhao, Y. Tsuchiya and N. Yabuuchi, *Small Methods*, 2019, **3**, 1800032.
- N. Yabuuchi, Y. Matsuura, T. Ishikawa, S. Kuze, J.-Y. Son, Y.-T. Cui, H. Oji and S. Komaba, *ChemElectroChem*, 2014, **1**, 580-589.
- K. Pan, H. Lu, F. Zhong, X. Ai, H. Yang and Y. Cao, *ACS Appl. Mater. Interfaces*, 2018, **10**, 39651-39660.